Model for scanning tunneling optical microscopy: A microscopic self-consistent approach

C. Girard
Laboratoire de Physique Moléculaire, Université de Besançon, 25030 Besancon CEDEX, France

D. Courjon
Laboratoire d'Optique P. M. Duffieux, Université de Besançon, 25030 Besancon CEDEX, France
(Received 7 March 1990)

A general method based on a microscopic picture of matter is developed in order to describe the optical interaction between a thin dielectric tip and a corrugated sample lighted in total reflection. Such a model is expected to interpret recent images obtained from scanning tunneling optical microscopy (steps, infinite tracks, glass plate with local scratches). The conversion of evanescent waves into homogeneous propagating ones is studied from a molecular-physics perspective (multipolar interactions between each atom of the tip and of the object). Our approach is concerned with the study of subwavelength details lying at the surface of a transparent medium. So, instead of solving the macroscopic Maxwell equations and applying the corresponding boundary conditions at the surface of the tip and of the object, we prefer a microscopic treatment in which the dielectric surrounding is taken into account from a set of dynamical matrices introducing all correlations between each elementary volume inside the object. Relations with experiments are discussed.

I. INTRODUCTION

In this paper we study the optical interaction between a dielectric tip and a corrugated surface lighted in total reflection. Our motivation in this work comes from recent experimental studies based on the use of local optical probes to image subwavelength structures lying on dielectric surfaces.[1-4] Indeed, a new type of optical microscopy has been recently developed. It is based on the detection of the near field lying in the vicinity of a dielectric surface.[5] In these experiments, the basic idea is to generate evanescent waves by total reflection at the surface of a transparent object and to detect the evanescent field by means of a dielectric stylus placed in a controlled way in the vicinity of the interface object air. This new scanning microscopy allows one to study individual nanometer size structures by trapping the near field generated by the matter. Such experiments carried out both in a constant-distance mode and a constant-intensity mode enable one to obtain images of steps and fractures appearing on mica and glass surfaces with a lateral resolution of 10 nm.

In order to use scanning tunneling optical microscopy not only for metrologic purposes, but also as a new physical probe, it is necessary to interpret these recent data. In the case of scanning near-field optical microscopy (SNOM) working in reflection mode, a recent theoretical study[6,7] has shown a dramatic dependence of the shape images on the polarization of the external field. In short, it seems that SNOM allows a better resolution of structures along the direction of polarization of the excitation field. The aim of this paper is to present a formalism that enables one to calculate the near field in the vicinity of various types of rough surfaces (stepped surface, little spheres adsorbed on transparent medium, etc.). There are various ways for describing the near field in the vicinity of an interface. Maxwell equations can be solved in specific cases where the boundary conditions can be easily defined.[8] On the other hand, another possibility consists of applying the diffraction theory or analyzing the diffracted field in term of angular spectrum. This approach leads to an interpretation in terms of propagating and evanescent waves.

A completely different way is based on a microscopic analysis of the light-matter interaction,[9-15] assuming discrete distribution of elementary components, each of them being characterized by a certain set of multipolar polarizabilities. This last approach will be developed in this paper. So, instead of solving the macroscopic Maxwell equations and of applying the corresponding boundary conditions at the surface limiting the tip and the sample, we prefer a microscopic treatment in which screening effects are taken into account from a dynamical self-consistent equation. Such a description introduces all correlations between n microsystems through a $(3n \times 3n)$ matrices. Note that similar methods, already used to study enhanced fields on rough surfaces and elastic scattering of light from small aggregates adsorbed on a flat-metal surface, open a new way for the understanding of the physical mechanisms appearing in optical microscopy by a local probe. Moreover, the microscopic approach[6] already applied for modeling SNOM foresees nanometer resolution and is not very far from the models developed in atomic force microscopy.[16-18] Another advantage of such a calculation lies in the possibility of simulating nanometer structures of arbitrary shape without introducing boundary conditions. In this case the generalized dielectric constant is built in the course of the calculation. Nevertheless, one must keep in mind that such an advantage is associated with a new computational difficulty connected to the great dimension of the dynamical matrix.

The paper will be organized as follows. In Sec. II we define a set of n self-consistent equations for each microsystem interacting individually with an evanescent wave generated above a transparent surface. The correlations between these systems are introduced in Sec. III, and Sec. IV is devoted to the study of the electric coupling with a spherical probe. Finally, numerical results of the detected intensity for various polarization of the excitation field and for various values of distance between tip and object will be given.

II. INTERACTION BETWEEN AN ISOLATED MICROSYSTEM AND AN EVANESCENT WAVE

We consider here the problem of a spherical microsystem (atom or molecule) placed above a local dielectric surface, as shown in Fig. 1. We calculate the effective field in the microsystem when an evanescent wave is generated in half the space $z>0$. We assume the approach distance d between the molecule and the surface is small compared with the wavelength λ of the emitted light in the dielectric ($z<0$). In this approximation, the interaction may be described from a set of nonretarded multipolar propagators defined by[19,20]

$$ {}^{(n)}\mathbf{S}^{(n')}(\mathbf{r},\mathbf{r}',\omega)=\frac{1}{2\pi}\left[\frac{\epsilon_0(\omega)-1}{\epsilon_0(\omega)+1}\right]\nabla_{r'}^{(n')}\nabla_{r}^{n'}G(\mathbf{r},\mathbf{r}') \tag{1}$$

with

$$ G(\mathbf{r},\mathbf{r}',\omega)=\int_{-\infty}^{+\infty}\int\frac{d\mathbf{k}}{k}f(\mathbf{l},z)f^{*}(\mathbf{l}',z') , \tag{2}$$

where $\mathbf{r}=(\mathbf{l},z)=(x,y,z)$ and $\epsilon_0(\omega)$ labels the dielectric constant of the surface. Moreover, we have

$$ f(\mathbf{l},z)=\exp(-i\mathbf{k}\cdot\mathbf{l}-kz) . \tag{3}$$

Note that for $n=n'=1$, one recovers the well-known expression of the dipolar propagator near a dielectric surface. The response of the microsystem will be described by its multipolar polarizabilities ${}^{(n)}\boldsymbol{\alpha}^{(n')}(\omega)$.[21] The spirit of the discussion will therefore be that the microsystem M and the dielectric are described by their responses to external fields (evanescent field and field generated by M).

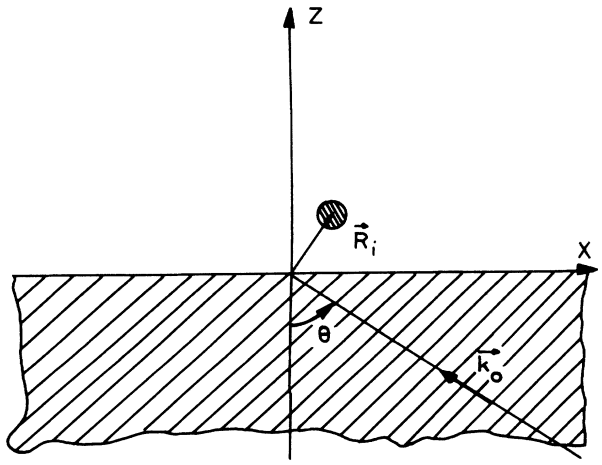

FIG. 1. A microscopic system labeled (i) interacts with an evanescent wave generated by total reflection in the dielectric medium: $\mathbf{k}_0$ characterizes the direction of the propagating wave.

A. The evanescent field in half the space $z>0$

Let us consider a plane wave falling on the boundary between two homogeneous media (air and glass interface). From classical boundary conditions, both transmitted and reflected waves simultaneously exist even in the case of total reflection.

If we call $k_0=n_0 2\pi/\lambda$ and $k_1=2\pi/\lambda$ the modulus of the propagation vectors in the transparent medium and in the air, respectively, and $n_0=\sqrt{\epsilon_0}$ the index of the refracting medium, the (K_x,K_y,K_z) components of the propagation vector $\mathbf{K}^T$ of the transmitted wave can be written

$$ \mathbf{K}^T=k_0[\sin\theta,0,i(\sin^2\theta-\sin^2\theta_L)^{1/2}] , \tag{4}$$

where θ is the incident angle and θ_L, the limit angle of refraction. $\mathbf{K}^T$ is then a complex vector whose real component k_x verifies the relation

$$ k_x=k_0\sin\theta\geq k_1 \quad \text{since } \theta\geq\theta_L . \tag{5}$$

The evanescent field is then given by

$$ \mathbf{E}_0(\mathbf{r},\omega)=(E_{ox}(\theta,k_0),E_{oy}(\theta,k_0),E_{oz}(\theta,k_0))\times\exp[i(\omega t-\mathbf{K}^T\cdot\mathbf{r})] . \tag{6}$$

Note that this expression will be taken as the zeroth-order solution of the self-consistent equation for the field at the level of the microsystem M.

B. The self-consistent equation for the field and the successive field gradients at the level of the microsystem (M)

When the microsystem (M) is placed in the vicinity of the dielectric surface, it is submitted to a set of effective-field gradients $\mathbf{E}^{(m)}(\mathbf{R},\omega)$. Its induced multipolar moments $\mathbf{m}^{(m)}(\omega)$ are given by the following relation:

$$ \mathbf{m}^{(m)}(\omega)=\sum_n\frac{1}{(2n-1)!!}{}^{(m)}\overleftrightarrow{\alpha}^{(n)}(\omega)[n]\mathbf{E}^{(n)}(\mathbf{R},\omega) , \tag{7}$$

where $\mathbf{R}$ represents the position vector of M and the symbol $[n]$ means a tensorial contraction between the tensors ${}^{(m)}\overleftrightarrow{\alpha}^{(n)}$ and $\mathbf{E}^{(n)}(\mathbf{R},\omega)$. Moreover, one has between the effective field $\mathbf{E}^{(1)}(\mathbf{R},\omega)$ and the successive field gradients the relation

$$ \mathbf{E}^{(n)}(\mathbf{R},\omega)=[\nabla_r^{(n-1)}\mathbf{E}^{(1)}(\mathbf{r},\omega)]_{\mathbf{r}=\mathbf{R}} . \tag{8}$$

In the framework of the linear response theory the nth-rank tensor $\mathbf{E}^{(n)}(\mathbf{R},\omega)$ may be expressed from the multipolar propagator ${}^{(n)}\mathbf{S}^{(m)}$. One has

$$\mathbf{E}^{(n)}(\mathbf{R},\omega)={}^{(n)}\mathbf{S}^{(m)}(\mathbf{R},\mathbf{R},\omega)[m]\mathbf{m}^{(m)}(\omega)+\mathbf{E}_0^{(m)}(\mathbf{R},\omega)\ , \tag{9}$$

where $\mathbf{E}_0^{(m)}(\mathbf{R},\omega)$ represents the mth-order gradient of the evanescent field $\mathbf{E}_0(\mathbf{R},\omega)$ [cf. Eq. (6)]. It is defined by

$$\mathbf{E}_0^{(m)}(\mathbf{R},\omega)=[\nabla_r^{(m-1)}\mathbf{E}_0(\mathbf{r},\omega)]_{\mathbf{r}=\mathbf{R}}\ . \tag{10}$$

The substitution of Eq. (7) into Eq. (9) leads to a self-consistent equation for the various field gradients experienced by the microsystem (M):

$$\mathbf{E}^{(n)}(\mathbf{R},\omega)=\sum_p \frac{1}{(2p-1)!}\,{}^{(n)}\mathbf{S}^{(m)}(\mathbf{R},\mathbf{R},\omega)[m] \times{}^{(m)}\vec{\vec{\alpha}}^{(p)}(\omega)[p]\mathbf{E}^{(p)}(\mathbf{R},\omega)+\mathbf{E}_0^{(n)}(\mathbf{R},\omega)\ . \tag{11}$$

Several remarks can be made about this result.

(i) If the charge distribution characterizing the system (M) is very localized (atoms or little molecules), the dipolar approximation is reasonable. In this case the multipolar polarizabilities ${}^{(m)}\vec{\vec{\alpha}}^{(p)}(\omega)$ of order (m and $p>1$) may be neglected. The self-consistent equation (11) becomes then

$$\mathbf{E}^{(1)}(\mathbf{R},\omega)=\mathbf{S}(\mathbf{R},\mathbf{R},\omega)\cdot\vec{\vec{\alpha}}(\omega)\cdot\mathbf{E}^{(1)}(\mathbf{R},\omega)+\mathbf{E}_0(\mathbf{R},\omega)\ , \tag{12}$$

where one has put $\vec{\vec{\alpha}}(\omega)\equiv{}^{(1)}\vec{\vec{\alpha}}^{(1)}(\omega)$ and ${}^{(1)}\mathbf{S}^{(1)}(\omega)\equiv\mathbf{S}(\omega)$ for the dipolar polarizability and the dipolar propagator. This equation can be easily solved by inverting a coupling matrix $\underline{A}(\mathbf{R},\omega)$

$$\mathbf{E}^{(1)}(\mathbf{R},\omega)=\underline{A}^{-1}(\mathbf{R},\omega)\cdot\mathbf{E}_0(\mathbf{R},\omega)\ . \tag{13}$$

Moreover from Eqs. (1) and (2), $\underline{A}(\omega)$ may be analytically calculated. We find

$$\underline{A}(\mathbf{R},\omega)=\begin{bmatrix} 1-\frac{f(\omega)}{8R^3} & 0 & 0 \\ 0 & 1-\frac{f(\omega)}{8R^3} & 0 \\ 0 & 0 & 1-\frac{f(\omega)}{4R^3} \end{bmatrix}, \tag{14}$$

with

$$f(\omega)=\alpha(\omega)\left[\frac{\epsilon_0(\omega)-1}{\epsilon_0(\omega)+1}\right]\ . \tag{15}$$

(ii) If now the spatial extension of the system M is important (little dielectric spheres, polyatomic molecule, etc.) the multipolar polarizabilities of higher order must be taken into account in the calculation of the effective field and in this case the more general equation (11) must be solved.

III. SELF-CONSISTENT EQUATION FOR AN ENSEMBLE OF N MICROSYSTEMS

When a great number of identical microsystems (atomic aggregate) interact with an external field (propagating or evanescent), the self-consistent field $\mathbf{E}(\mathbf{R}_i,\omega)$ on each atomic site can be determined from a $(3n\times 3n)$ matrice equation. In the case of systems of weak spatial extension, the effective fields $\mathbf{E}(\mathbf{R}_i,\omega)$ and $\mathbf{E}(\mathbf{R}_j,\omega)$ acting on two microsystems (i) and (j) are related by the following self-consistent equation:

$$\mathbf{E}(\mathbf{R}_i,\omega)=\mathbf{E}^{(1)}(\mathbf{R}_i,\omega)+\sum_{j\neq i}\mathbf{T}(\mathbf{R}_i-\mathbf{R}_j)\cdot\vec{\vec{\alpha}}(\omega)\cdot\mathbf{E}(\mathbf{R}_j,\omega)\ . \tag{16}$$

Within the dipolar approximation $\mathbf{E}^{(1)}(\mathbf{R}_i,\omega)$ is given by the relation (13) and the retarded propagator $\mathbf{T}$ in the vacuum is defined by[22]

$$\mathbf{T}(\mathbf{R}_i-\mathbf{R}_j)=\exp\left[-i\frac{\omega}{c}|\mathbf{R}_i-\mathbf{R}_j|\right]\left[\mathbf{T}_3(\mathbf{R}_i-\mathbf{R}_j)+\frac{i\omega}{c}\mathbf{T}_2(\mathbf{R}_i-\mathbf{R}_j)-\frac{\omega^2}{c^2}\mathbf{T}_1(\mathbf{R}_i-\mathbf{R}_j)\right]\ . \tag{17}$$

The second-rank tensors $\mathbf{T}_3$, $\mathbf{T}_2$, and $\mathbf{T}_1$ are given by

$$\mathbf{T}_3(\mathbf{r})=\frac{3\mathbf{r}\mathbf{r}-r^2\mathbf{I}}{r^5}\ , \tag{18}$$

$$\mathbf{T}_2(r)=\frac{3\mathbf{r}\mathbf{r}-r^2\mathbf{I}}{r^4}\ , \tag{19}$$

and

$$\mathbf{T}_1(\mathbf{r})=\frac{\mathbf{r}\mathbf{r}-r^2\mathbf{I}}{r^3}\ , \tag{20}$$

where $\mathbf{I}$ represents the identity tensor. It is important to note that, when the spatial extension of the aggregate is small with respect to the wavelength λ, the radiative term of $\mathbf{T}(\mathbf{R}_1-\mathbf{R}_j)$ may be disregarded. Now, in order to solve Eq. (16), it is convenient to introduce two supervectors defined by

$$\vec{\mathbf{E}}^{(1)}(\omega)=(\mathbf{E}^{(1)}(\mathbf{R}_1,\omega),\mathbf{E}^{(1)}(\mathbf{R}_2,\omega),\ldots,\mathbf{E}^{(1)}(\mathbf{R}_n,\omega)) \tag{21}$$

and

$$\vec{\mathbf{E}}(\omega)=(\mathbf{E}(\mathbf{R}_1,\omega),\mathbf{E}(\mathbf{R}_2,\omega),\ldots,\mathbf{E}(\mathbf{R}_n,\omega))\ .$$

The relation (16) becomes then

$$\vec{\mathbf{E}}(\omega)=\vec{\mathbf{E}}^{(1)}(\omega)+\alpha(\omega)\underline{B}(\omega)\cdot\vec{\mathbf{E}}(\omega)\ , \tag{22}$$

where $\underline{B}(\omega)$ represents a $(3n\times 3n)$ matrix:

$$\underline{B}(\omega)=\begin{bmatrix} 0\ 0\ 0 & & & \\ 0\ 0\ 0 & \mathsf{T}(\mathbf{R}_1-\mathbf{R}_2) & \mathsf{T}(\mathbf{R}_1-\mathbf{R}_3) & \cdots \\ 0\ 0\ 0 & & & \\ & 0\ 0\ 0 & & \\ \mathsf{T}(\mathbf{R}_2-\mathbf{R}_1) & 0\ 0\ 0 & \mathsf{T}(\mathbf{R}_2-\mathbf{R}_3) & \cdots \\ & 0\ 0\ 0 & & \\ & & 0\ 0\ 0 & \\ \mathsf{T}(\mathbf{R}_3-\mathbf{R}_1) & \mathsf{T}(\mathbf{R}_3-\mathbf{R}_2) & 0\ 0\ 0 & \cdots \\ & & 0\ 0\ 0 & \\ \vdots & \vdots & \vdots & \end{bmatrix}, \quad (23)$$

where the vanishing terms on the diagonal express the fact that it is not possible to couple a given microsystem with itself. The solution of Eq. (22) can be written in a very compact way:

$$\vec{\mathbf{E}}(\omega)=[\mathsf{I}-\alpha(\omega)\underline{B}(\omega)]^{-1}\cdot\vec{\mathbf{E}}^{(1)}(\omega) . \quad (24)$$

The matrix $[\mathsf{I}-\alpha(\omega)\underline{B}(\omega)]$ describing the electric coupling between every microsystem plays a central role in our formalism. In the near-field range, we will show that it contains subwavelength features of the object.

IV. OPTICAL INTERACTION WITH A DIELECTRIC TIP

The conversion of evanescent waves into homogeneous ones can be performed with a dielectric stylus placed in the vicinity of the object. In other words, the nonhomogeneous field generated by the surface can be then locally converted into a propagating mode by optical tunneling. This section aims to detail such physical mechanisms. The stylus playing the role of detector will be represented as a sphere of radius a. This choice avoids the complexity due to the conical shape of the probe used in experiments. Nevertheless, it retains the main characters of the physical process studied here. Note that a complete description of the probe shape could be taken into account from a microscopic treatment similar to those used in Sec. III to characterize the aggregate. Such improvements are left for a further step. In this section we restrict our purpose by considering the probe as a continuum medium characterized by an isotropic dipolar susceptibility $\chi_p(\omega)$.

A. The self-consistent equation for the dipole moment induced in the probe extremity

In the absence of detector the field generated by the surface is given by

$$\mathbf{E}_t(\mathbf{r},\omega)=\mathbf{E}_0(\mathbf{r},\omega)+\sum_{i=1}^{n}\mathsf{T}(\mathbf{r}-\mathbf{R}_i)\cdot\vec{\alpha}(\omega)\cdot\vec{\mathbf{E}}(\mathbf{R}_i,\omega) , \quad (25)$$

where $\vec{\mathbf{E}}(\mathbf{R}_i,\omega)$ represents the self-consistent field acting on the ith microsystem, i.e., it is the ith component of the supervector $\mathbf{E}(\omega)$ given by Eq. (24). When the probe is placed in the vicinity of the surface, its extremity is submitted to $\mathbf{E}_t$. Consequently, it acquires a fluctuating dipole moment $\boldsymbol{\mu}(\omega)$. This dipole can be again described from a self-consistent relation including the response of the object:

$$\boldsymbol{\mu}(\mathbf{R}_p,\omega)=\boldsymbol{\mu}_0(\mathbf{R}_p,\omega)+g(\omega)\chi_p(\omega)\int_v[\mathsf{S}(\mathbf{r},\mathbf{R}_p,\omega)+\mathsf{S}_{ag}(\mathbf{r},\mathbf{R}_p,\omega)]\times\boldsymbol{\mu}(\mathbf{R}_p,\omega)d\mathbf{r} , \quad (26)$$

where $\mathbf{R}_p$ represents the position vector of the center of the sphere, S is given, in the nonretarded approximation, by Eq. (1); S_{ag} represents the dipolar propagator associated to the atomic aggregate, and $\boldsymbol{\mu}_0(\mathbf{R}_p,\omega)$ defines the first-order-induced dipole, i.e., in other words, the direct interaction of $\mathbf{E}_t$ with the tip. This term may be obtained by performing a spatial integration on a little sphere of radius a and of susceptibility $\chi_p(\omega)$:

$$\boldsymbol{\mu}_0(\mathbf{R}_p,\omega)=g(\omega)\chi_p(\omega)\int_v\mathbf{E}_t(\mathbf{r},\omega)d\mathbf{r} \quad (27)$$

in which v represents the volume of the sphere and $g(\omega)$ defines a screening factor connected to the continuous treatment used to describe the tip:

$$g(\omega)=\frac{3}{3+4\pi\chi_p(\omega)} . \quad (28)$$

Moreover, in a first approximation, when one disregards the possible many-body contributions involving the high-order interactions between several atoms belonging to the aggregate, it is possible to write the dipolar propagator $\mathsf{S}_{ag}(\mathbf{r},\mathbf{r}',\omega)$ as a simple sum of microscopic contributions

$$\mathsf{S}_{ag}(\mathbf{r},\mathbf{r}',\omega)=\sum_{i=1}^{n}\mathsf{T}(\mathbf{r}-\mathbf{R}_i)\cdot\vec{\alpha}(\omega)\cdot\mathsf{T}(\mathbf{R}_i-\mathbf{r}') . \quad (29)$$

Note that such an approximation may be justified by the fact that S_{ag} appears in the perturbative term of Eq. (26) only.

B. Signal detected by the tip

Now, in order to solve Eq. (26), it is convenient to introduce the following (3×3) matrix:

$$\underline{C}(\mathbf{R}_p,\omega)=\mathsf{I}-g(\omega)\chi_p(\omega)\int_v[\mathsf{S}(\mathbf{r},\mathbf{R}_p,\omega)+\mathsf{S}_{ag}(\mathbf{r},\mathbf{R}_p,\omega)]d\mathbf{r} . \quad (30)$$

This quantity, which describes the dynamical coupling between the detector and the object of interest, depends on the dimension of the stylus extremity through the spatial integration of $d\mathbf{r}$. It will be calculated in Appendix A. We have then

$$\boldsymbol{\mu}(\mathbf{R}_p,\omega)=\underline{C}^{-1}(\mathbf{R}_p,\omega)\cdot\boldsymbol{\mu}_0(\mathbf{R}_p,\omega) . \quad (31)$$

This dipole scatters in the upper part of the tip a propagating wave of intensity proportional to

$$\mathbf{I}(\mathbf{R}_p)=\frac{\omega^4}{c^4}|\mathsf{T}_1(\mathbf{R}_{0b}-\mathbf{R}_p)\cdot\underline{C}^{-1}(\mathbf{R}_p,\omega)\cdot\boldsymbol{\mu}_0(\mathbf{R}_p,\omega)|^2 . \quad (32)$$

From this general relation, it is possible to build a tridimensional map of a defect (track, step, microscopic monocrystal, etc.) lying on a planar infinite surface.

Before going beyond and in order to clarify the further discussions, we summarize the more important points appearing in the preceding sections. First, we recall that the detected intensity $\mathbf{I}(\mathbf{R}_p)$ is the relevant quantity in experimental studies presented in Refs. 2–5. Thus, a numerical analysis of $\mathbf{I}(\mathbf{R}_p)$ needs the following procedure.

Determination of the evanescent field $\mathbf{E}_0$ in half the space ($z>0$). This vector represents the zeroth order of the self-consistent problem.

Research of a self-consistent equation for the field at each ith atomic site of a surface exhibiting nanometric roughness. From Eqs. (13), (14), and (24) this field is given by

$$\vec{\mathbf{E}}(\mathbf{R}_i,\omega)=\sum_{j=1}^{n}[\underline{M}^{-1}(\omega)]_{\mathbf{R},\mathbf{R}}\underline{A}^{-1}(\mathbf{R}_j,\omega)\cdot\mathbf{E}_0(\mathbf{R}_j,\omega) \tag{33}$$

in which the $(3n\times 3n)$ matrix $\underline{M}(\omega)$ is defined by

$$\underline{M}(\omega)=\mathbf{I}-\vec{\boldsymbol{\alpha}}(\omega)\underline{B}(\omega) \tag{34}$$

and finally, determination of both the matrix $\underline{C}(\mathbf{R}_p,\omega)$ and the vector $\boldsymbol{\mu}_0(\mathbf{R}_p,\omega)$ (cf. Appendixes A and B).

V. NUMERICAL RESULTS

In this section we present numerical calculations based on relations (32), (A4), (A7), (B3), and (B4). We have chosen some typical systems (MgO, NaCl, etc.) of nanometer sizes lying on a perfectly planar dielectric surface (mica) (a single atomic system, an aggregate of few atoms, and one or several infinite tracks). In a first step, we define different dielectric functions useful to describe the object. The atomic polarizability of each atom forming the aggregate may be described from a Drude oscillator model.[23] One has then

$$\alpha(\omega)=\frac{\alpha_a(0)\omega_a^2}{\omega_a^2-\omega^2}\ , \tag{35}$$

where $\alpha_a(0)$ and ω_a represent the static polarizability and the effective frequency of the oscillator, respectively. The dynamic properties of the planar substrate will be characterized by the following optical dielectric constant:

$$\epsilon(\omega)=1+\beta\left[1-\left[\frac{\omega}{\omega_0}\right]^2\right]^{-1}. \tag{36}$$

For the mica the constants β and ω_0 are equal to 1.483 and 0.38 a.u., respectively.[23] From these relations, we have calculated the intensity $I(\mathbf{R}_p)$ detected above several kinds of objects (cf. Figs. 2–5). Moreover, one has chosen a polarization parallel to the (oy) axis for the incident wave propagating inside the transparent medium. Some important remarks may be made about these numerical results.

(i) Figure (2) gives a tridimensional representation of the intensity $I(\mathbf{R}_p)$ detected after scanning of an area of

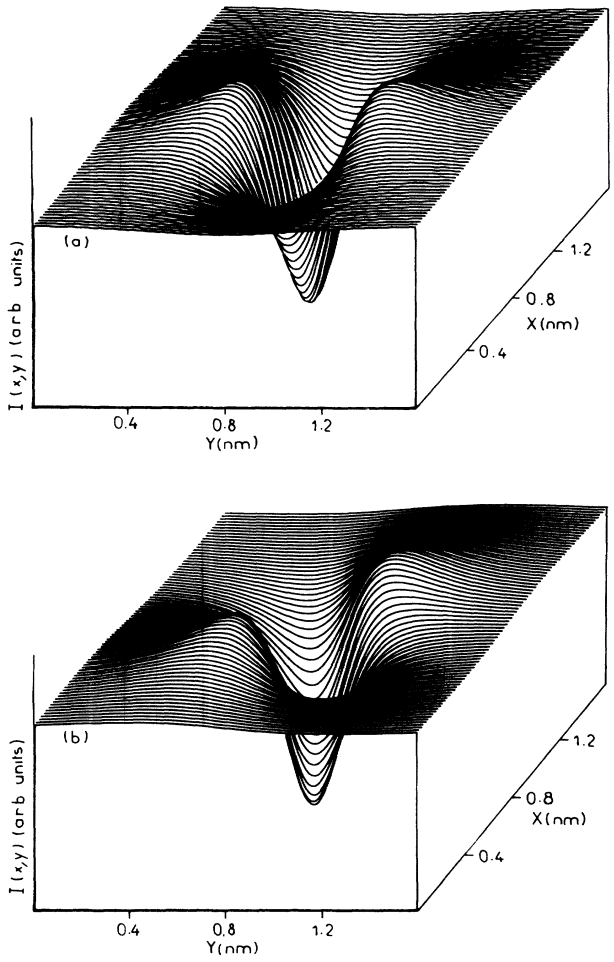

FIG. 2. Tridimensional representation of the detected intensity $I(x,y)$ calculated with a probe whose extremity reduces to a sphere of radius $a=0.25$ nm. The object is a spherical polarizable system adsorbed on a planar dielectric surface: (a) The direction of the incident beam is given by $\mathbf{k}_0=(k_x,k_y,k_z)$, with $k_x=k_y$. (b) The direction of the incident beam is defined by $\mathbf{k}_0=(k_x,k_y,k_z)$, with $k_x=k_y$.

1.61×1.6 nm^2 above a single polarizable system (s) for which $\alpha_a=1.5$ Å^3. The most important feature of this map is that the intensity decreases when the probe is just above the system (s). This behavior may be explained simply by examinating the sign of near-field dipolar propagator $\mathsf{T}_3(\mathbf{r},\mathbf{r}')$ between the scattering microscopic system and the center of the probe. In fact, when the detector overhangs the system (s), the near field generated is then in phase opposition with the one of the evanescent field. Consequently the microscopic object(s) appears in contrast reversal. Note that such a contrast differs from the one obtained in reflection near-field microscopy[6,7] in which the near field is generated by the extremity of the dielectric stylus. What is more, it may be seen on Fig. 2 that the polarization of the external field $\mathbf{E}_0(\omega)$ introduces an anisotropy in the image of an initially spherical system. In our case (TE mode), the confinement of the object is better in the (Oy) direction [cf. Fig. 2(a)].

(ii) In order to study the influence of the correlations between the different microscopic systems belonging to a same atomic aggregate, we give in Fig. 3 both the image calculated by taking into account the effects due to the correlation matrix $\underline{B}(\omega)$ (solid curves) and the one calculated by neglecting this contribution (dashed curves). In this case, the object is a small aggregate of (7×7) atoms of identical dipolar polarizability $\alpha_a=1.5$ Å^3. This aggregate is adsorbed on a planar surface at a distance $D_a=3$ Å. The profile image along the (Oy) axis is given for three different values of the interatomic distance d_a between each scattering center. One remarks that for an interatomic distance d_a greater than 4 Å and by using the value $\alpha_a=1.5$ Å^3, the dipolar correlations becomes negligible [cf. Fig. 3(a)]. On the other hand, when d_a decreases and becomes close to about 2 Å, the profile of the aggregate is very sensitive to the dipolar correlations. In this case [Fig. 3(c)] the profile of the aggregate evolves and becomes like the one of a single dipole. To summarize, at the realistic interatomic distance $d_a\simeq3$ Å, the surrounding effect appears as a little correction in the near-field calculation. This behavior is due to the rapid spatial dependence (like R^{-3}) of the nonradiative term mediated by the tensor $T_3(\mathbf{r},\mathbf{r}')$ and to the small extension of the aggregate. Note that this property is not true in far-field range where the dipolar centers are correlated on longer distances.

(iii) Figure 4 represents the surface map of the intensity $I(\mathbf{R}_p)$ detected by a very thin probe ($a=0.4$ nm) scanning a planar surface exhibiting an infinite track in the (Ox) direction. The track of width $b=6.2$ nm and height $c=2.4$ nm is formed of a great number of atoms separated by a distance $d_a=3$ Å. Moreover the images 4(a), 4(b), and 4(c) have been calculated for three values of the nearest approach distance $\tilde{d}=R_{pz}-a-b$. At any distance R_{pz}, the object appears, as in Fig. 2, in contrast reversal. Moreover Fig. 4(a) shows that at very short range, the rectangular shape of the track is well restored with a very thin tip. At a longer approach distance [Figs. 4(b) and 4(c)] the object appears less well defined spatially but remains detectable. In any case, these results clearly show that the near field detected at a very small distance from a corrugated object contains subwavelength details lying on a dielectric surface.

(iv) In order to complete our numerical study we have examined how the images of several parallel tracks evolve when the tip-object distance d increases. Figures 5 and 6 give the image of five tracks of identical height $c=9$ nm and of width $b=10.8$ nm. Each track is separated by a gap e equal to 8 nm. The object appears well defined for $0.25\leq\tilde{d}\leq3$ nm (Fig. 5). Beyond this limit value the image of five tracks becomes equivalent to the one of a single track of width $b_{eq}=5b+4e$.

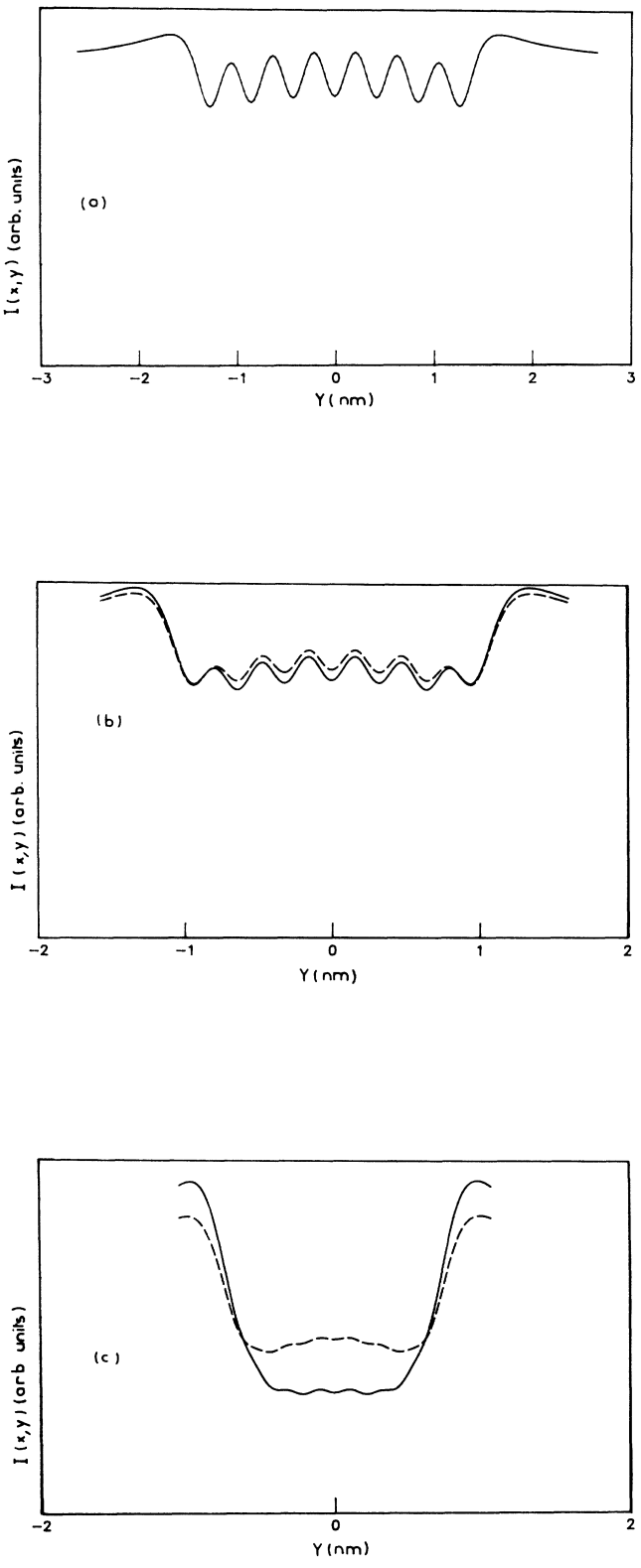

FIG. 3. Numerical study of the influence of the dipolar correlations on the detected intensity $I(0,y)$. The object is a small aggregate of (7×7) atoms lying on a planar surface. Solid curves and dashed curves represent both calculations performed by including the dipolar interactions and by neglecting the dipolar interactions; $a=0.25$ nm and $R_{pz}=1$ nm. (a) The interatomic distance $d_a=0.4$ nm. (b) $d_a=0.3$ nm. (c) $d_a=0.2$ nm.

VI. CONCLUSION

We have presented a microscopic self-consistent approach to describe the optical interaction between a thin

dielectric tip and a corrugated surface lighted in total reflection. In the near-field range the interaction is described in terms of multipolar localized interactions. When the probe is placed at some nanometers to the surface, the images calculated from this method exhibit features of nanometer size and show in this case a possibility to overpass the Rayleigh limit. Moreover, when it is submitted to an external excitation (evanescent wave), each polarizable system confines a nonradiative field in a very small spatial region. The extension of this field depends on the magnitude of the dipolar polarizability. The first cause of confinement is the rapid decreasing of the near field generated by each dipolar center. Moreover, along the direction parallel to the external field, a

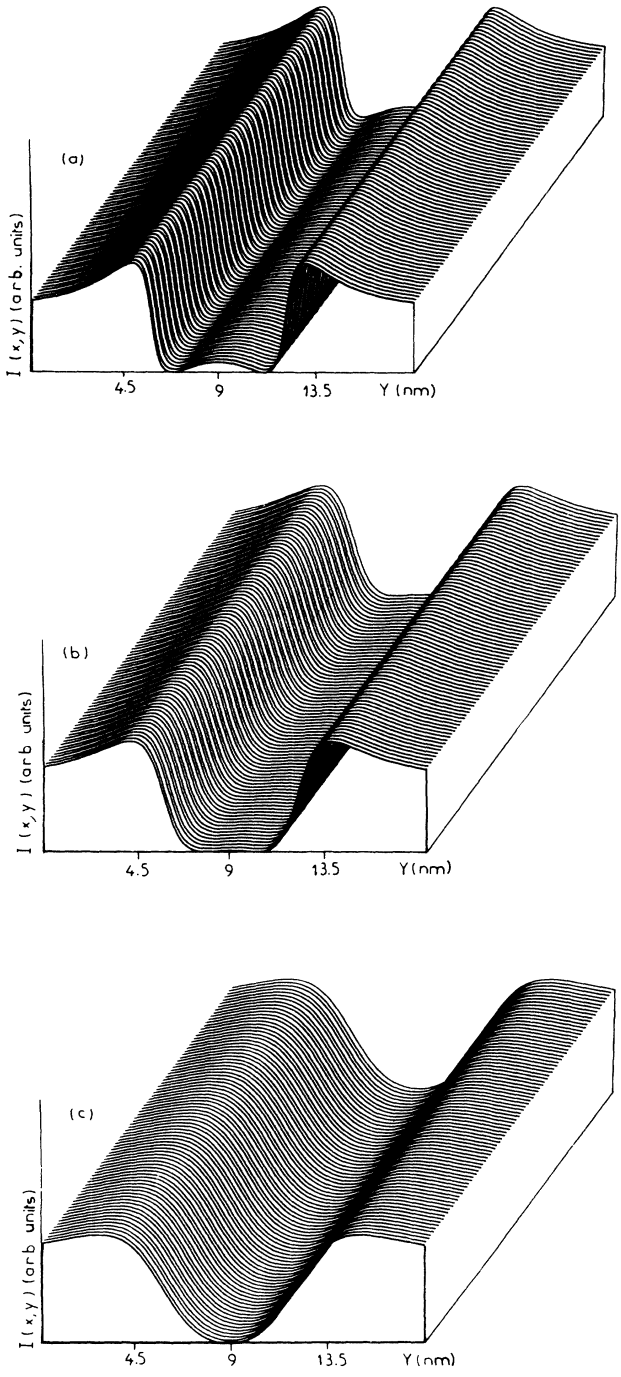

FIG. 4. Tridimensional representation of the intensity $I(x,y)$ detected by a spherical probe of radius $a=0.4$ nm. We have chosen an infinite track of height $c=2.4$ nm and of width $b=6.2$ nm. (a) The nearest approach distance $\bar{d}=R_{pz}-a-b$ is equal to 0.35 nm. (b) $\bar{d}=1$ nm. (c) $\bar{d}=2.35$ nm.

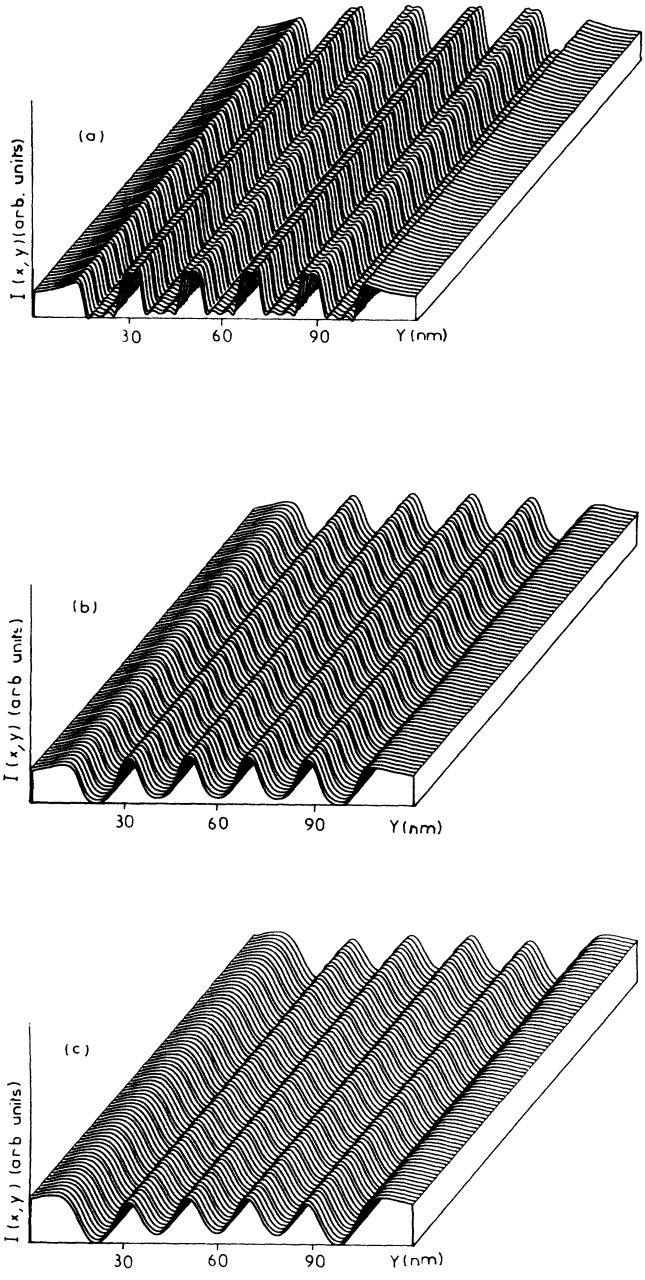

FIG. 5. Tridimensional calculated map of a perfectly planar surface exhibiting five infinite tracks of identical height $c=9$ nm. The tracks have a width $b=10.3$ nm and are separated by a gap of width $e=8$ nm. (a) The size of the tip extremity is chosen equal to $a=1$ nm and $\bar{d}=0.25$ nm. (b) Same object with $a=1$ nm and $\bar{d}=1.25$ nm. (c) Same object with $a=1$ nm and $\bar{d}=1.75$ nm.

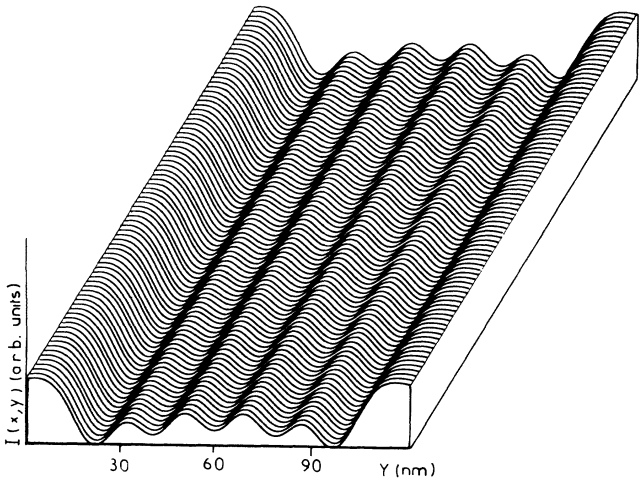

FIG. 6. Same caption as Fig. 5 for $\bar{d}=3.75$ nm. In this case the image becomes similar to that of a larger track of width equal to $5b+4e$.

phenomenon of "overconfinement" appears due to the change of sign of near field when the tip moves above a microscopic system. Consequently, in this direction a given dipole appears as a hole of very small width.

Rectangular tracks have been modeled as a set of polarizable atoms. In this case, the shape of the image also appears in contrast reversal and at very short approach distance the edge of the track is very well restored. Concerning the influence of the second nonradiative term of dependence like R^{-2}, calculations indicate that the corresponding contribution can be neglected at small tip-sample distances used in experimental studies.

Finally, as it stands, our model could also be used to investigate local plasmon resonances appearing near metallic aggregate deposed on a planar transparent surface (mica, for example). Such a calculation which needs to take into account the nonlocal effects introduced by the delocalized electrons moving in the aggregate will be performed by applying the present method and nonlocal theory developed in Ref. 24.

ACKNOWLEDGMENTS

The authors would like to express their sincere thanks to Professors D. Van Labeke and J. M. Vigoureux for a number of stimulating discussions. The Laboratoire de Physique Moléculaire is "unite Associée au Centre National de la Recherche Scientifíque No. 772." The Laboratoire d'Optique P. M. Duffieux is "unite associée au Centre National de la Recherche Scientifique No. 214."

APPENDIX A: CALCULATION OF THE MATRIX $C(\mathbf{R}_p,\omega)$

From Eq. (30), the coupling matrix between the sample and the tip can be separated into two contributions connected to the perfectly planar surface and to the aggregate, respectively:

$$\underline{C}(\mathbf{R}_p,\omega)=\underline{1}-\bar{\underline{C}}(\mathbf{R}_p,\omega)+\tilde{\underline{C}}(\mathbf{R}_p,\omega)\ , \qquad \mathbf{R}_p=(R_{px},R_{py},R_{pz}) \tag{A1}$$

with

$$\bar{\underline{C}}(\mathbf{R}_p,\omega)=g(\omega)\chi_p(\omega)\int_v \mathbf{S}(\mathbf{r},\mathbf{R}_p,\omega)d\mathbf{r} \tag{A2}$$

and

$$\tilde{\underline{C}}(\mathbf{R}_p,\omega)=g(\omega)\chi_p(\omega)\int_v \mathbf{S}_{ag}(\mathbf{r},\mathbf{R}_p,\omega)d\mathbf{r}\ . \tag{A3}$$

In the near-field range, these matrices may be obtained from the relations (1) and (29). After integration on the sphere involving straightforward calculations one obtains analytical expressions for $\bar{\underline{C}}$,

$$\bar{\underline{C}}(\mathbf{R}_p,\omega)=-2\pi a h(\omega)\frac{1}{R_{pz}}\begin{bmatrix} 1+\dfrac{a^2}{12R_{pz}^2} & & \\ 0 & 1+\dfrac{a^2}{12R_{pz}^2} & \\ 0 & 0 & -\left[1-\dfrac{a^2}{12R_{pz}^2}\right] \end{bmatrix} \tag{A4}$$

with

$$h(\omega)=g(\omega)\chi_p(\omega)\left[\frac{\epsilon_0(\omega)-1}{\epsilon_0(\omega)+1}\right]\ . \tag{A5}$$

1. The corrugation part of the matrix $\underline{C}$

In the same way: the corrugation part of $\underline{C}$ can be analytically calculated:

$$\tilde{\underline{C}}(\mathbf{R}_p,\omega)=g(\omega)\chi_p(\omega)\sum_{i=1}^{n}\mathbf{J}(\mathbf{R}_i)\cdot\tilde{\underline{\alpha}}(\omega)\cdot\mathbf{T}(\mathbf{R}_i-\mathbf{R}_p)\ , \tag{A6}$$

where

$$\mathbf{J}(\mathbf{R}_i)=\int_v d\mathbf{r}\,\mathbf{T}(\mathbf{r}-\mathbf{R}_i),\ \mathbf{R}_i=(\mathbf{l}_i,z_i)=(x_i,y_i,z_i)\ . \tag{A7}$$

Note that at short range corresponding to $|\mathbf{R}_p|<\lambda$, one can neglect the radiative contribution in the expression of the propagator $\mathbf{T}$. If moreover the radius of the sphere is

small with respect to λ, one may write

$$\exp[-i(\omega/c)|\mathbf{R}_p-\mathbf{R}_i|]\simeq 1 \ . \tag{A8}$$

One has then

$$\mathbf{J}(\mathbf{R}_i)=\mathbf{J}_3(\mathbf{R}_i)+\frac{i\omega}{c}\mathbf{J}_2(\mathbf{R}_i) \tag{A9}$$

with

$$\mathbf{J}_3(\mathbf{R}_i)=\int_v d\mathbf{r}\,\mathbf{T}_3(\mathbf{r}-\mathbf{R}_i) \tag{A10}$$

and

$$\mathbf{J}_2(\mathbf{R}_i)=\int_v d\mathbf{r}\,\mathbf{T}_2(\mathbf{r}-\mathbf{R}_i) \ . \tag{A11}$$

2. The tensors $\mathbf{J}_3$ and $\mathbf{J}_2$

In order to calculate these tensors it is more appropriate to work in a particular frame (X,Y,Z) in which $\mathbf{J}_3$ and $\mathbf{J}_2$ are diagonal. This frame will be labeled F_R and the matrix $\underline{R}$ used to return to the absolute frame F_r is a function of two Euler angles (φ,θ) referring to the orientation of the vector $(\mathbf{R}_p-\mathbf{R}_i)$ with respect to F_r. The definition of the angles is that of Rose:[25]

$$\underline{R}(\varphi,\theta)=\begin{bmatrix}\cos\varphi\cos\theta & -\sin\varphi & \cos\varphi\sin\theta\\ \sin\varphi\cos\theta & \cos\varphi & \sin\varphi\sin\theta\\ -\sin\theta & 0 & \cos\theta\end{bmatrix} \ . \tag{A12}$$

In this expression the cosine and the sine of φ and θ may be expressed as a function of the components of $\mathbf{R}_p$ and $\mathbf{R}_i$ as

$$\cos\varphi=\frac{R^x_{p,i}}{l_i}, \quad \sin\varphi=\frac{R^y_{p,i}}{l_i} \tag{A13}$$

and

$$\cos\theta=\frac{R_p-z_i}{R_{p,i}}, \quad \sin\theta=\frac{l_i}{R_{p,i}} \tag{A14}$$

with

$$\mathbf{l}_i=(R_{p,x}-x_i,R_{py}-y_i)$$

and (A15)

$$\mathbf{R}_{p,i}=(\mathbf{l}_i,R_{pz}-z_i) \ .$$

Let us write the expression $\mathbf{J}_3$ and $\mathbf{J}_2$ in the reference F_R,

$$\mathbf{J}'_3=\begin{bmatrix}J'_{3xx} & 0 & 0\\ 0 & J'_{3yy} & 0\\ 0 & 0 & J'_{3zz}\end{bmatrix}, \tag{A16}$$

$$\mathbf{J}'_2=\begin{bmatrix}J'_{2xx} & 0 & 0\\ 0 & J'_{2yy} & 0\\ 0 & 0 & J'_{2zz}\end{bmatrix} \ . \tag{A17}$$

In the absolute frame F_r, these tensors can be expressed by the following transformation equations:

$$[\mathbf{J}_3(\mathbf{R}_i)]_{ij}=R_{ik}R_{ji}[\mathbf{J}'_3(\mathbf{R}_i)]_{kl} \tag{A18}$$

and

$$[\mathbf{J}_2(\mathbf{R}_i)]_{ij}=R_{ik}R_{jl}[\mathbf{J}'_2(\mathbf{R}_i)]_{kl} \tag{A19}$$

in which the matrix $\underline{R}$ appears twofold since we transform here second-rank tensors.

Thus, from these final expressions, it is possible to express in a simple way the corrugation matrix $\tilde{C}$ defined by the Eq. (A6) as

$$\tilde{C}(\mathbf{R}_p,\omega)=\alpha(\omega)g(\omega)\chi_p(\omega)\sum_{i=1}^{n}\left[\mathbf{J}_3(\mathbf{R}_i)+\frac{i\omega}{c}\mathbf{J}_2(\mathbf{R}_i)\right]\left[\mathbf{T}_3(\mathbf{R}_i-\mathbf{R}_p)+\frac{i\omega}{c}\mathbf{T}_2(\mathbf{R}_i-\mathbf{R}_p)\right], \tag{A20}$$

where $\mathbf{T}_3$ and $\mathbf{T}_2$ are given in the absolute frame F_r from Eqs. (18) and (19).

APPENDIX B: THE ZEROTH-ORDER-INDUCED DIPOLE MOMENT $\boldsymbol{\mu}_0(\mathbf{R}_p,\omega)$

It remains now, to determine the vector $\boldsymbol{\mu}_0(\mathbf{R}_p,\omega)$ induced in the tip. Following the same procedure as the one presented in Appendix A, we separate $\boldsymbol{\mu}_0(\mathbf{R}_p,\omega)$ into two different parts:

$$\boldsymbol{\mu}_0(\mathbf{R}_p,\omega)=\bar{\boldsymbol{\mu}}_0(\mathbf{R}_p,\omega)+\tilde{\boldsymbol{\mu}}_0(\mathbf{R}_p,\omega) \ . \tag{B1}$$

Thus, as in Eq. (A1), $\bar{\boldsymbol{\mu}}_0(\mathbf{R}_p,\omega)$ represents the continuum contribution generated by the evanescent wave only:

$$\bar{\boldsymbol{\mu}}_0(\mathbf{R}_p,\omega)=g(\omega)\chi_p(\omega)\int_V \mathbf{E}_0(\mathbf{r},\omega)d\mathbf{r} \tag{B2}$$

and $\tilde{\boldsymbol{\mu}}_0(\mathbf{R}_p,\omega)$ is due to the nanometer structures lying on the surface

$$\tilde{\boldsymbol{\mu}}_0(\mathbf{R}_p,\omega)=g(\omega)\chi_p(\omega)\alpha(\omega)\sum_{i=1}^{n}\int\mathbf{T}(\mathbf{r}-\mathbf{R}_i)\cdot\mathbf{E}(\mathbf{R}_i,\omega)d\mathbf{r} \ .$$

The integration over the sphere can be performed from the previous results developed in Appendix A [Eqs. (A7), (A10), and (A11)] to yield

$$\tilde{\boldsymbol{\mu}}_0(\mathbf{R}_p,\omega)=g(\omega)\chi_p(\omega)\alpha(\omega)\times\sum_{i=1}^{n}\left[\mathbf{J}_3(\mathbf{R}_i)+\frac{i\omega}{c}\mathbf{J}_2(\mathbf{R}_i)\right]\cdot\mathbf{E}(\mathbf{R}_i,\omega) \tag{B3}$$

and

$$\bar{\boldsymbol{\mu}}_0(\mathbf{R}_p,\omega)=\bar{\boldsymbol{\alpha}}_p(\omega)F(a)\mathbf{E}_0(\mathbf{R}_p,\omega) \ , \tag{B4}$$

where $\bar{\alpha}_p(\omega)$ denotes the dipolar polarizability of the tip

$$\alpha_p(\omega)=\frac{4\pi}{3}a^3\chi_p(\omega)g(\omega) \tag{B5}$$

and $F(a)$ defines a shape factor describing the spatial extension of the spherical extremity of the probe. It is given by

$$F(a)=\frac{3}{4a^3}\left[e^{K_z a}\left[\frac{2a}{K_z^2}-\frac{2}{K_z^3}\right]+e^{-K_z a}\left[\frac{2a}{K_z^2}+\frac{2}{K_z^3}\right]\right]. \tag{B6}$$

We study now a limit case deduced from this last result. When the radius a of the sphere becomes very small, the factor $F(a)$ may be expanded on series as

$$F(a)\simeq\frac{3}{4a^3}\left[\frac{2a}{K_z^2}(2+K_z^2a^2)-\frac{2}{K_z^2}\left[2K_z a+\frac{K_z^a}{3}a^3\right]\right]. \tag{B7}$$

Thus when $a\to 0$, $F(a)=1$, and in this case one recovers the result obtained in the framework of the dipolar approximation:

$$\bar{\mu}_0(R_p,\omega)=\alpha_p(\omega)\mathbf{E}_0(R_p,\omega)\equiv\alpha_p(\omega)\mathbf{E}_0(\theta,k_0)e^{-k_z R}. \tag{B8}$$

[1]D. W. Pohl, W. Denk, and M. Lanz, Appl. Phys. Lett. **44**, 651 (1984).

[2]R. Reddick, R. J. Warmack, and T. L. Ferrell, Phys. Rev. B **39**, 767 (1989).

[3]D. Courjon, K. Sarayeddine, and M. Spajer, Opt. Commun. **71**, 23 (1989).

[4]F. De Fornel, J. P. Goudonnet, L. Salomon, and E. Lesniewska, ECO2 Optical Storage Scanning Technology, **1139**, 77 (1989).

[5]D. Courjon, J. M. Vigoureux, M. Spajer, K. Sarayeddine, and S. Leblanc, Appl. Opt. (to be published).

[6]B. Labani, C. Girard, D. Courjon, and D. Van Labeke, J. Opt. Soc. Am. B **7**, 936 (1990).

[7]C. Girard and M. Spajer, Appl. Opt. (to be published).

[8]J. Goodman, *Introduction To Fourier Optics* (McGraw-Hill, New York, 1968).

[9]M. J. Renne, and B. R. A. Nijboer, Chem. Phys. Lett. **1**, 317 (1967).

[10]J. Lekner and P. J. Castle, Physica A **101**, 89 (1980).

[11]M. Meier, A. Wokaun, and F. P. Liao, J. Opt. Am. B **2**, 931 (1985).

[12]A. Wokaun, Mol. Phys. **56**, 1 (1985).

[13]O. Keller and B. Sonderkaer, SPIE Optical Testing Metrology **959**, 344 (1988).

[14]A. Johner, R. Schaaf, and A. Schmitt, J. Opt. **19**, 207 (1988).

[15]A. Johner and R. Schaaf, Phys. Rev. B **40**, 10 231 (1989).

[16]G. Binning, C. F. Quate, and C.H. Gerber, Phys. Rev. Lett. **56**, 930 (1986).

[17]C. Girard, D. Van Labeke, and J. M. Vigoureux, Phys. Rev. B **40**, 12 133 (1989).

[18]D. Van Labeke, B. Labani, and C. Girard, Chem. Phys. Lett. **162**, 399 (1989).

[19]C. Girard and C. Girardet, J. Chem. Phys. **86**, 6531 (1987).

[20]C. Girard and L. Galatry, Surf. Sci. **141**, L338 (1984).

[21]A. D. Buckimgham, Adv. Chem. Phys. **12**, 107 (1967).

[22]B. Linder and D. A. Rabenold, Adv. Chem. Phys. **6**, 203 (1972).

[23]J. Mahanty and B. W. Ninham, *Dispersion Forces* (Academic, London, 1976).

[24]G. Girard, S. Maghezzi, and F. Hache, J. Chem. Phys. **91**, 5509 (1989).

[25]M. E. Rose, *Elementary Theory of Angular Momentum* (Wiley, New York, 1967).